1.E.3:
1.E.4

Nuclear Physics **A344** (1980) 294–306;

MEASUREMENT OF THE g-FACTOR AND LIFETIME OF THE FIRST-EXCITED STATE OF ^{20}O

A. J. RUTTEN, A. HOLTHUIZEN, J. A. G. DE RAEDT †, W. A. STERRENBURG and G. VAN MIDDELKOOP ††

Fysisch Laboratorium, Rijksuniversiteit Utrecht, PO Box 80.000, Utrecht, The Netherlands

Received 21 March 1980

Abstract: The g-factor and mean lifetime of the first-excited 2^+ state at 1.67 MeV in ^{20}O have been determined by means of a plunger set-up. The state was populated by the ^{3}H(^{18}O, pγ)^{20}O reaction at $E(^{18}\text{O}) = 24.5$ MeV. The analysis of p-γ anisotropies as a function of flight path of the recoiling ion in vacuum leads to a value for the g-factor of $|g| = 0.352 \pm 0.015$ and to a mean life of $\tau = 10.7 \pm 0.4$ ps.

E NUCLEAR REACTION ^{3}H(^{18}O, pγ), $E = 24.5$ MeV; measured p$\gamma(\theta)$ vs. product flight time in vacuum. ^{20}O level deduced g, $T_{1/2}$. Enriched target. Plunger technique.

1. Introduction

Accurate measurements of nuclear g-factors form in many cases a severe test of nuclear wave functions. For three even-A oxygen isotopes the g-factors of the first-excited states have been determined [1–6]) with errors of 5 % for ^{16}O and ^{18}O and 10 % for ^{20}O. The results for the first two isotopes are well reproduced by shell-model calculations with Kuo-Brown matrix elements [7]). A similar calculation for ^{18}O with modified matrix elements by Chung [8]), however, is off by many standard deviations. For ^{20}O the Chung matrix elements reproduce the known value [6]) ($|g| = 0.39 \pm 0.04$) quite well, whereas a shell-model calculation by Arima *et al.* [9]) apparently yields much too small a value, $g \simeq -0.15$. Experimentally the sign of the g-factor for $^{20}\text{O}(2_1^+)$ has been determined to be negative [10]). From calculations based on simple pure configurations and the experimental value for ^{18}O one also expects a rather small negative value ($g \simeq -0.2$) for ^{20}O.

Values for the mean lifetime of this state are clearly in mutual disagreement. A recoil-distance measurement performed simultaneously with the above-mentioned g-factor experiment [6]) yielded $\tau = 14.2 \pm 0.8$ ps, whereas a Doppler-shift attenuation

† Present address: Department of Nuclear Physics, University of Oxford, England.
†† Present address: Natuurkundig Laboratorium, Vrije Universiteit, Amsterdam, The Netherlands.

measurement [11]) yielded $\tau = 9.8 \pm 0.7$ ps. It has been suggested by Hermans *et al.* [11]) that this apparent discrepancy might be due to a slight, presumably slow, $4_1^+ \rightarrow 2_1^+$ γ-ray feeding in the singles recoil-distance work. If this were true it may also have affected the g-factor determination [6]).

It was therefore thought worthwhile to determine the g-factor of the 2_1^+ state of ^{20}O with good precision with the coincident time-differential recoil-into-vacuum method [1]). At the same time the mean life of this state can be accurately measured.

2. Experimental procedure

The time-differential recoil-into-vacuum method makes use of the very strong static magnetic hyperfine interaction in highly ionized atoms recoiling at high velocities in vacuum. Due to this hyperfine interaction the initially aligned spin of the excited nuclear state is periodically deoriented. This effect is observed by means of a plunger set-up [1, 12]), as a time-dependent oscillation in the anisotropy of γ-rays deexciting the nuclear state.

The first-excited 2^+ state of ^{20}O at 1.67 MeV was populated by means of the $^3H(^{18}O, p)^{20}O$ reaction at a bombarding energy of 24.5 MeV. At this energy the anisotropy of the p-γ angular correlation has a maximum for proton detection at 0° to the beam direction (see fig. 1). This bombarding energy also provides sufficient recoil velocity for the final nucleus ($v/c = 0.039$) so that a significant fraction of the

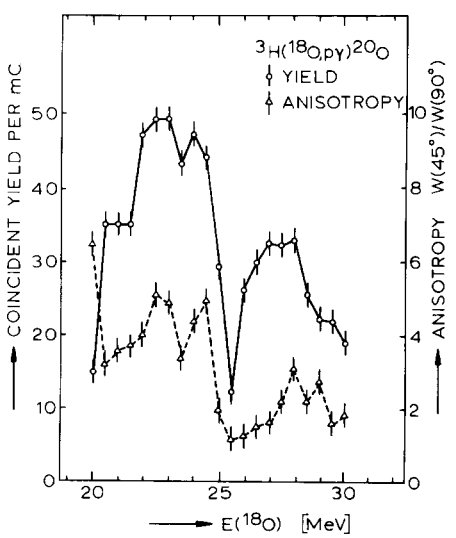

Fig. 1. Coincident yield and anisotropy for the $^3H(^{18}O, p_1\gamma)$ reaction. The yield is averaged over two 12.7 cm diam. × 12.7 cm long NaI(Tl) detectors at 45° and 90° to the beam direction and at 16 cm from the 100 μg/cm^2 Ti-^{3}H target, for protons detected at 0° with a solid angle of 50 msr, and is given per mC collected charge. In this experiment the target layer was facing the beam.

nuclear ions are produced as hydrogen-like ions, which yield the strongest hyperfine interaction.

2.1. THE DETECTOR SET-UP

Gamma-rays were detected in six 12.7 cm diameter by 12.7 cm long NaI(Tl) detectors and a large-volume Ge(Li) detector, in coincidence with protons. Four scintillation detectors were positioned in a horizontal plane at angles $\pm 45°$ and $\pm 90°$ to the beam direction and two detectors were placed at angles of 45° with the horizontal plane and at $\pm 90°$ to the beam direction. They were all placed at 16 cm from the beam spot on the target. The 125 cm^3 Ge(Li) detector was positioned at 0° to the beam direction and at a distance of 13.5 cm.

Protons were detected at 0° to the beam direction in a 2 mm thick Si surface-barrier detector subtending a solid angle of 50 msr. The Si detector was shielded by a 90 μm thick Au foil to stop the primary ^{18}O beam.

2.2. TARGET PREPARATIONS

A target of hydrated (^3H) titanium was produced by NUKEM at Hanau (W. Germany). It consists of a 1 μm thick nickel foil with a layer of 300 $\mu g/cm^2$ Ag evaporated onto one side to improve the heat conduction. A Ti layer of 100$\mu g/cm^2$ was evaporated onto the other side of the nickel foil over an area with a diameter of 3.5 mm. The Ti was hydrated with ^3H by heating the foil to a temperature of about 400 °C in a ^3H atmosphere. In this way a compound is formed with 95 ^3H atoms per 100 Ti atoms. In this process the titanium structure is blown up appreciably, which causes the originally smooth target surface to become rough.

The targets were delivered in pre-stretched form mounted on a ring, which fitted on the target holder of the plunger (see below).

2.3. THE PLUNGER

The plunger system will be described elsewhere [13]). Therefore only details relevant to the present work are given. It consists of two essentially identical conventional foil stretchers [14]), one mounted in a fixed position (the target) and one mounted on a sleigh (the stopper). The target foil can be adjusted so as to be parallel to the stopper foil. The sleigh is positioned by means of an inchworm † [see also ref. [13])], a rod of which the position is accurately controlled by three piezo-electric crystals.

The back of each foil is viewed by a laser interferometer. For this purpose the laser beam of a He-Ne laser (λ = 632 nm), mounted outside the vacuum chamber of the plunger system, is split into two beams, which in turn are split into a beam

† Burleigh Instruments Inc., East Rochester, NY, USA.

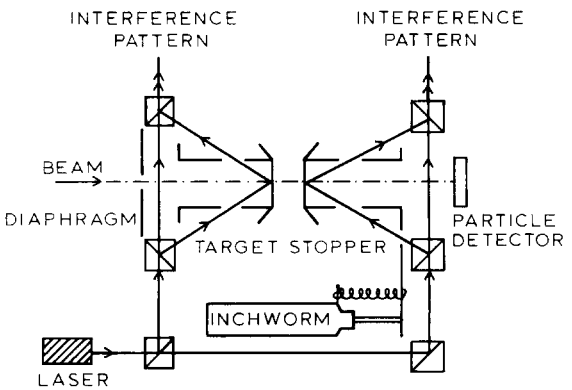

Fig. 2. Schematic drawing of the plunger set-up showing the inchworm drive of the stopper and the light paths of laser beams in two interferometers. The interference pattern from the stopper foil, formed outside the vacuum chamber, was used for distance measurements, and that from the target for visual inspection.

reflected at the back of the target foil (or stopper foil) and a direct reference beam. The pairs of interfering beams are projected, outside the chamber, through a simple lens system onto a screen to form a visible interference pattern (see fig. 2). The pattern of the stopper foil is also viewed by light sensitive diodes connected to a fringe-counting system. In this way the relative position of the stopper foil can be measured to an accuracy of 0.2 μm. Simultaneously the capacity of the condenser formed by the two foils is measured as an independent check. Two reference points are used in the positioning procedure, electrical contact of the foils, and a fixed far-distance point. Positioning during the run was found to be reproducible to within 5 fringes, i.e. to 1.0 μm.

It was found that the distance of closest approach (electrical contact between the stopper and the target) was about 50 μm due to the imperfections of the target foil (see subsect. 2.2). This distance was estimated independently from an extrapolation of the measured plunger capacity [see also ref. [14])], from the measured γ-ray anisotropy as a function of foil separation (see subsect. 3.2), as well as from the recoil-distance lifetime measurement (see subsect. 3.4).

2.4. EXPERIMENTAL CONDITIONS

The experiment was performed with the Ti-^{3}H layer facing the stopper. Therefore the ^{18}O beam had to penetrate the Ag and Ni layers before hitting the ^{3}H target. It was found experimentally that the incident energy of the ^{18}O ions should be 26.0 MeV to produce the desired energy of 24.5 MeV at the ^{3}H target. During the experiment the current of the $^{18}O^{5+}$ ion beam, produced with the Utrecht 6 MV Van de Graaff tandem accelerator, was maintained at 50 ± 10 nA to avoid excessive

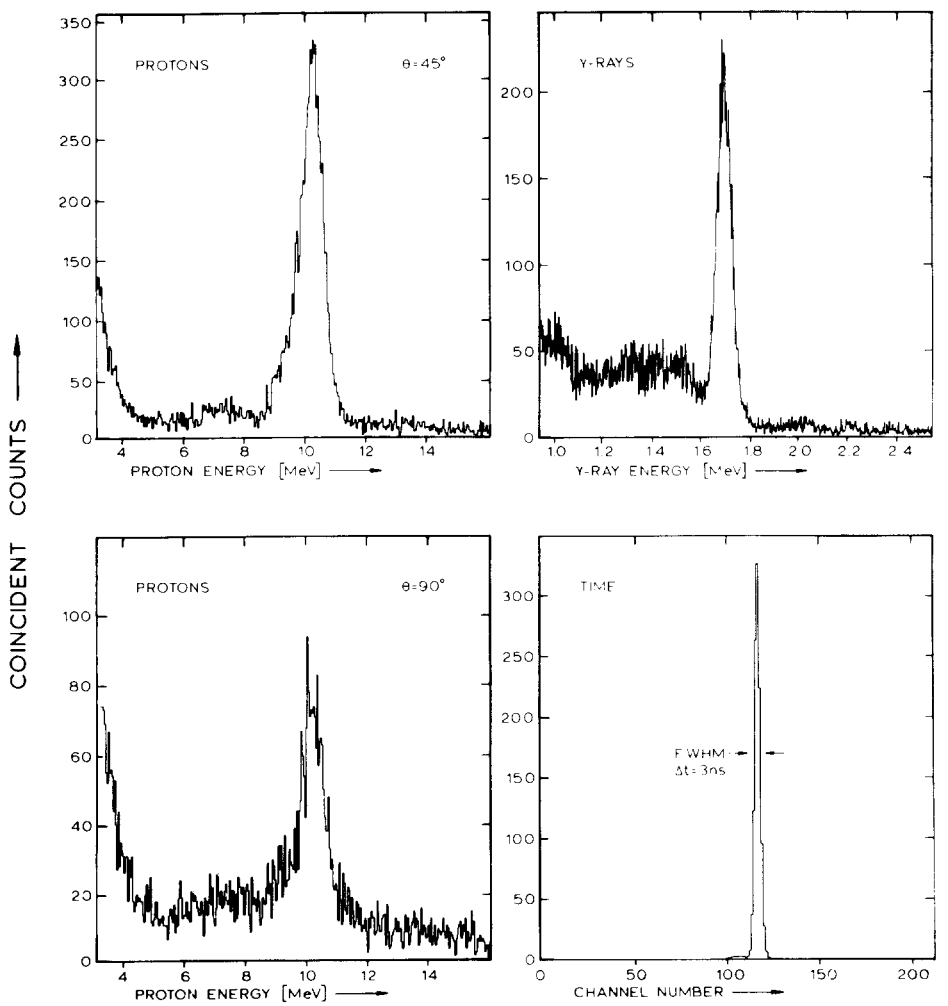

Fig. 3. Typical proton spectra coincident with γ-ray photo-peaks measured at θ_γ = 45° and 90°, a coincident γ-ray spectrum and a time spectrum. The displayed spectra represent sums over several runs.

heating of the target and stopper foils. The shift of the stopper foil between beam-on and -off was found to be less than two fringes (0.4 μm).

After the experiment a run was performed on the stopper foil only to check the amount of target material transferred to the stopper. This amount was found to be negligible.

Data were taken by means of an on-line PDP 11/40 computer system. Events, consisting of digitized pulse heights from the seven γ-ray detectors, the particle detector and the corresponding "timing detectors" (time-to-amplitude converters), were written on magnetic tape for later off-line analysis. Typical coincident proton,

γ-ray and time spectra are shown in fig. 3. It appeared that during the runs there was a considerable build-up of carbon on the target. By properly gating the coincident spectra, however, the background due to this build-up could be greatly suppressed in the final analysis; see subsect. 3.1.

3. Results

3.1. THE g-FACTOR MEASUREMENT

The coincident photo-peak intensities $W(\theta)$ of the 1.67 MeV γ-rays at $\theta = 90°$ and 45° to the beam direction were calculated as follows. Due to carbon build-up on the target there was a considerable coincident background from the $^{12}C(^{18}O, pn)$ ^{28}Al reaction. This background appeared in the particle spectrum as a continuous, practically linear proton spectrum. For this reason the analysis was performed on the peaks in the particle spectra corresponding to γ-ray photopeaks events in the γ-ray spectra. The net numbers of coincidences were obtained by subtracting appropriately weighted numbers of counts in particle windows just below and just above the particle peak from those in the peak window.

The measured anisotropy, i.e. $R = W(90°)/W(45°)$ as a function of the plunger distance is given in fig. 4. The point at zero distance in fig. 4 was obtained in a separate measurement on a different target. The anisotropy was measured with the stopper far away and later with a stopper at zero distance, which consisted of a 12 mg/cm^2

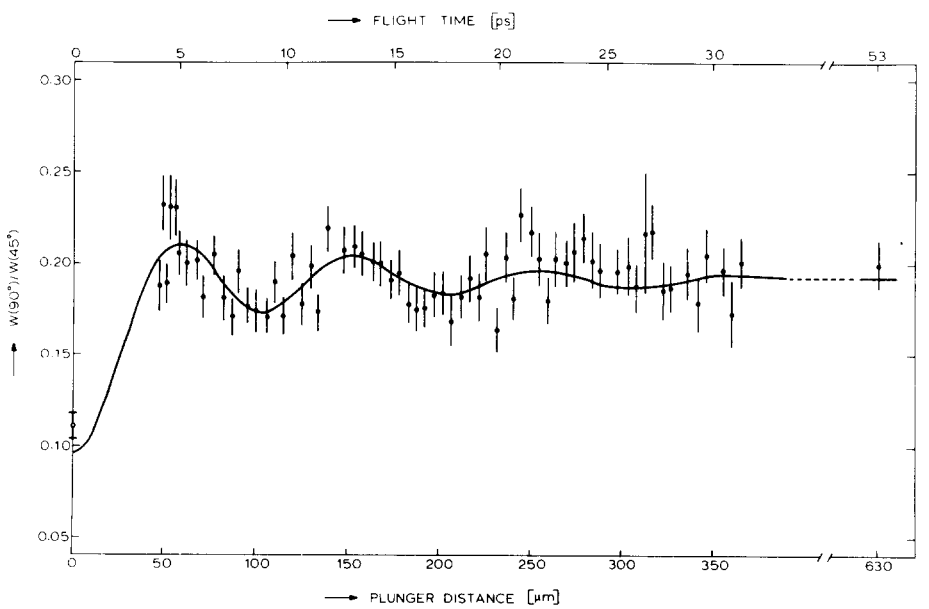

Fig. 4. The time-dependent γ-ray anisotropy $W(90°)/W(45°)$ measured with the plunger. The curve represents the best fit to the data; see text. The zero-distance point (open circle) was not used in this fit.

thick Ag layer evaporated directly onto the target. The ratio of these anisotropies was found to be 1.73 ± 0.09, which in combination with the fitted anisotropy at far distance (see fig. 4 and subsect. 3.2) leads to a value for the zero-distance point of $W(90°)/W(45°) = 0.111 \pm 0.007$.

3.2. INTERPRETATION

The ^{20}O ions recoil out of the target foil into vacuum with a measured velocity of $v = (0.0393 \pm 0.0006)c$ (see subsect. 3.4). This leads to a calculated equilibrium distribution for single-electron, two- and three-electron ions in vacuum of 26, 49 and 21 %, respectively [15]). The main contributions of the static hyperfine interaction to the perturbation of the γ-ray angular correlation stem from electron configurations with an unpaired 1s electron. These configurations are obviously the ground state of the single-electron ions and excited states of two- and three-electron ions.

In table 1 we have listed the single- and two-electron configurations with mean lives comparable to or larger than the nuclear lifetime. Only those configurations may contribute to the hyperfine interaction in free ions. The $^1S_0$ and $^3P_0$ terms have been omitted since they yield no hyperfine interaction. The ground state and excited-state three-electron configurations have interaction strengths comparable to that of the $(2s)^1$ and those of the $(1s)^1(2s)^1$ or $(1s)^1(2p)^1$ configurations, respectively. For this reason three-electron configurations have not been taken into account explicitly. Because the mean lives of the ^2P terms (see table 1) are short compared to the nuclear lifetime also these terms have been omitted in the analysis.

The time-dependent perturbation of the γ-ray angular correlation $W(\theta)$ as measured with the plunger method is described by the coefficient $G_k(t)$, defined

TABLE 1

Single- and two-electron configurations with contributions to the hyperfine interaction in isolated ions

Configuration	Term	Mean life	Interaction [a])
Single-electron ions			
$(1s)^1$	$^2S_{1/2}$	∞	s
$(2s)^1$	$^2S_{1/2}$	460 ns [b])	w
$(2p)^1$	$^2P_{1/2,\,3/2}$	0.4 ps [b])	w
Two-electron ions			
$(1s)^1(2s)^1$	$^3S_1$	1.3 ms [c])	s
$(1s)^1(2p)^1$	$^3P_1$	1.5 ns [d])	s
	$^3P_2$	6.3 ns [c])	s

[a]) Hyperfine interaction denoted by strong (s) and weak (w) have strengths of the order of that of the $(1s)^1$ configuration and of an order of magnitude weaker, respectively.
[b]) Ref. [16]). [c]) Ref. [17]). [d]) Ref. [18]).

by eq. (5) of ref. [12]), in the expression

$$W(\theta, t) = \sum_{k=0,2,4} G_k(t) Q_k A_k P_k(\cos\theta). \quad (1)$$

In this equation Q_k, A_k and P_k denote the finite γ-ray detector attenuation coefficients, the unperturbed angular correlation coefficients and Legendre polynomials, respectively. The coefficients $G_k(t)$ contain the interaction angular frequencies $\omega^i_{FF'}$ for each contributing term i defined by

$$\omega^i_{FF'} = \frac{1}{\hbar}(E^i_F - E^i_{F'}) = \{F(F+1) - F'(F'+1)\}\frac{a^i_J}{2\hbar} g, \quad (2)$$

where F, F' denote the total angular momentum, i.e. the vector sum of the nuclear spin I and the atomic spin J, a^i_J is the corresponding interaction energy [19]) and g is the nuclear g-factor. Depending on J there can be more than one angular frequency per term. The coefficients $G_k(t)$ are a sum over contributions from each term weighted by its relative population α_i; they also depend on the nuclear lifetime τ.

The interaction energies a^i_J were obtained from values given in ref. [12]). In this way all frequencies $\omega^i_{FF'}$ can be related to $\omega_0 \equiv \omega_{\frac{5}{2},\frac{3}{2}}$ for the $(1s)^1$ configuration. This implies that the nuclear g-factor can be deduced from the measured time-differential anisotropy essentially by using eq. (1), in which the parameters τ, ω_0 and α_i are varied to obtain the best fit to the experimental data points. In addition, the distance of closest approach d_0 between target and stopper was taken as an adjustable parameter (see subsect. 3.3).

The least-squares fit (with a normalized χ^2 of 1.1) leads to the values for the parameters that are given in table 2. It should be noted that the values found for α_i may be too low because of the rough surface of the target. This results in flight path variations for the ions, which in turn leads to an attenuation of the measured anisotropy variation as a function of flight path. Therefore no conclusions should be drawn from the comparatively low α_i values for the excited two-electron states [see e.g. ref. [20])]. The errors given in table 2 correspond to standard deviations. In subsect. 3.3 we evaluate the error in the g-factor, by considering the uncertainties in all contributing parameters.

TABLE 2

Measured parameters deduced from a least-squares fit to the data

Quantity [a])	Value	Quantity [a])	Value [c])
ω_0	0.719 ± 0.018 ps^{-1}	$\alpha\{^2S_{1/2}, (2s)^1\}$	(5 ± 2) %
τ [b])	10.3 ± 0.8 ps	$\alpha\{^3S_1\}$	(4 ± 4) %
d_0	47 ± 3 μm	$\alpha\{^3P_1\}$	(4 ± 4) %
$\alpha\{^2S_{1/2}, (1s)^1\}$	(11 ± 2) %	$\alpha\{^3P_2\}$	(6 ± 3) %

[a]) For the meaning of the symbols see text.
[b]) In the final analysis $\tau = 10.7 \pm 0.4$ ps has been used (see subsects. 3.3 and 3.4).
[c]) For the $^3S_1$ and $^3P_{1,2}$ terms a statistical distribution has been taken.

3.3. ERROR ANALYSIS

The total error in the g-factor consists of contributions from uncertainties in a number of parameters and of course depends on counting statistics. Although some parameters are correlated the total error is calculated by a quadratic addition of the contributions to the uncertainty in the g-factor due to standard deviations in the various parameters. This is a reasonable procedure since in the computer analysis of the data (see fig. 4) a simultaneous linear least-squares fit was performed for all contributing hyperfine frequencies, whose relative values are fixed by the well known interaction energies [see e.g. ref. [12])], for a number of values for g, d_0 and τ. The values for d_0 and τ were determined independently such that the effect on the g-factor of their uncertainties could be determined by varying their values within the error limits. The various contributions to the error in the g-factor are discussed below (see also table 3).

TABLE 3

Summary of the contributions to the relative error in the g-factor

Source of error	Contribution to error (%)
statistics	2.6
zero distance	2.3
lifetime	0.3
recoil velocity	1.5
two-electron analysis [a])	1.6
total error	4.1

[a]) From ref. [12]).

3.3.1. The zero distance. The zero distance (point of electrical contact between target and stopper) was determined independently in two ways. It was estimated from the measurement of the plunger capacity as a function of distance by extrapolation to be $d_0 = 48 \pm 3$ μm. The distance d_0 was also used as an adjustable parameter in the fit of the mean lifetime of the 2_1^+ state (see subsect. 3.4) and was found to be $d_0 = 45 \pm 3$ μm. In the fit of the g-factor to the measured time-dependent γ-ray anisotropy (fig. 4) the minimum χ^2 was obtained for $d_0 = 47 \pm 3$ μm. Since these values are in good mutual agreement we have adopted $d_0 = 47 \pm 3$ μm as an *independent* value for the zero distance. It should be noted that the error is a conservative estimate. The contribution of this uncertainty to the relative error in g was determined by letting d_0 vary between 44 and 50 μm in the g-factor fit with fixed values for the other parameters; this yields a contribution of ± 2.3 % (see table 3).

3.3.2. The lifetime τ. The value for τ was taken from the lifetime measurement; see subsect. 3.4. Again the contribution to the error in the g-factor was obtained by ranging τ within plus and minus one standard deviation, which leads to a ± 0.3 % variation in g.

3.3.3. The initial velocity v. The initial velocity was determined from the coincident γ-ray spectra measured simultaneously with the Ge(Li) detector at 0° to the beam direction (see subsect. 3.4). This velocity v is a direct measure of the time scale and hence of the g-factor. Therefore the relative error in v (± 1.5 %) leads to an identical contribution to the error in g.

3.3.4. The two-electron analysis. The contribution of the uncertainty in this analysis to the error in g is taken from ref. [12]) where the appropriate arguments are given. This contribution amounts to ± 1.6 %.

The relative errors obtained in this way were combined with the statistical error (2.6 %) and lead to a total uncertainty of 4.1 % in the value of the g-factor. The value of ω_0 finally leads to a g-factor of $|g| = 0.352 \pm 0.015$.

3.4. THE LIFETIME MEASUREMENT

The γ-rays were counted in a 125 cm^3 Ge(Li) detector coincident with protons detected in a Si surface barrier detector. Both detectors were positioned at 0° to the beam axis. The net numbers of coincident "flight" and "stopped" γ-rays were obtained after an appropriate background correction. In the total coincident γ-ray spectrum taken by the Ge(Li) detector (see fig. 5a) four peaks are observed in the 1600–1800 keV energy interval. The 1634 keV γ-ray corresponds to the 1.63 → 0 MeV transition in ^{20}Ne produced in the β-decay of ^{20}F, which is formed by the ^{3}H(^{18}O, n) ^{20}F reaction. The 1779 keV γ-ray is due to the ^{28}Al β-decay following the ^{12}C(^{18}O, pn)^{28}Al reaction. These lines disappear by properly gating on protons corresponding to the ^{20}O(2_1^+) state. The remaining two lines (see figs. 5a and b) correspond to γ-rays from the ^{20}O 1.67 → 0 MeV transition detected in flight and after stopping of the recoiling ^{20}O ions, respectively.

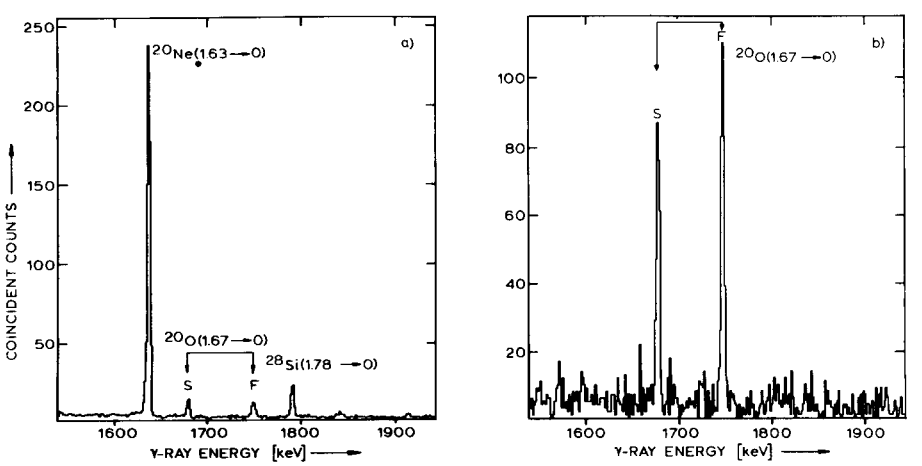

Fig. 5. A total coincident γ-ray spectrum taken with the Ge(Li) at 0° to the beam direction (a) and a γ-ray spectrum gated with protons corresponding to the 2_1^+ state of ^{20}O (b).

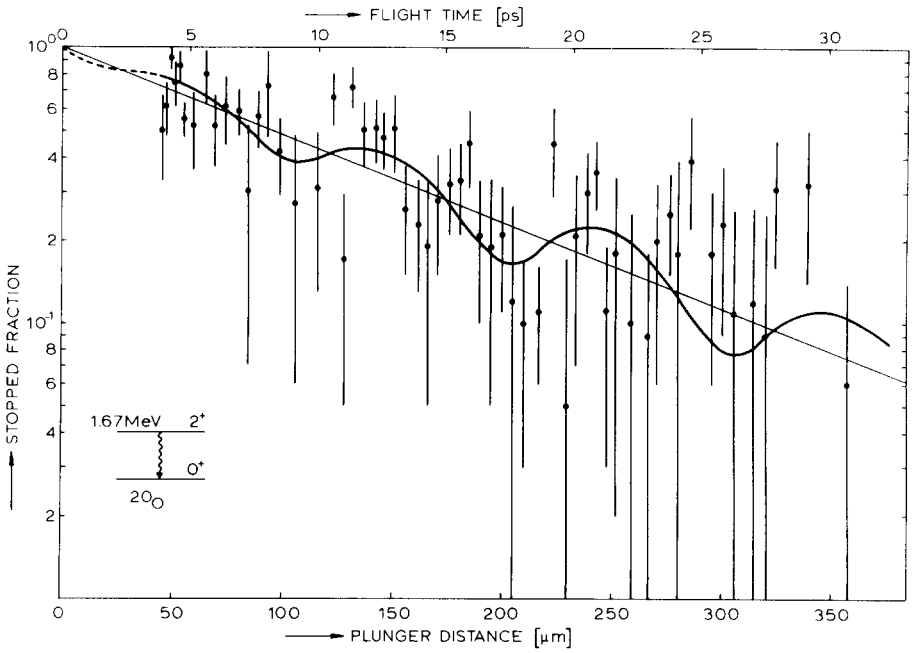

Fig. 6. Fraction of $^{20}O(2_1^+)$ nuclei decaying in the stopper, $I_s/(I_s+I_f)$, as a function of the plunger distance. The curve is a best fit for a superposition of the exponential decay and deorientation (see text).

The energy separation of the photopeaks corresponding to γ-rays emitted in flight and emitted after the nuclei have slowed down in the stopper was found to be 65.3 ± 0.6 keV. The energy calibration was obtained from the photopeak positions of the unshifted 1633.7 ± 0.3 keV ^{20}Ne γ-ray [21]) and the "stopped" 1673.7 ± 0.2 keV ^{20}O γ-ray [21]). Together with corrections for the γ-ray detector opening angle (19°) and for relativistic effects the energy separation between "stopped" and "flight" peaks leads to a recoil velocity of $v = (0.0393\pm0.0006)c$ for the excited ^{20}O ions in vacuum.

The measured stopped fraction, i.e. the number of photopeak counts I_s for the "stopped" 1.67 MeV γ-ray divided by the number of photopeak counts I_s+I_f in the "stopped" and "flight" γ-rays together, is given as a function of plunger distance d in fig. 6. These data were fitted by the commonly used expression

$$I_s/(I_s+I_f) = \exp\{-(d+d_0)/v\tau\} \tag{3}$$

with superposition of the spin-deorientation effect. This effect can be computed in a straightforward fashion from the numbers given in table 2. Parameters in the fit are τ and d_0. The least-squares fit (with a normalized χ^2 of 1.4) leads to a mean life and zero distance of $\tau = 10.7\pm0.4$ ps and $d_0 = 45\pm3$ μm, respectively. Both values are in good agreement with those found from the analysis of the g-factor measurement; see subsect. 3.2.

4. Conclusion

In table 4 we have listed the known experimental values for the magnetic dipole moments of the first-excited states of even O-isotopes together with the available theoretical predictions. Unfortunately none of the theoretical papers reports calculations for all three isotopes. The Kuo-Brown calculations [7]) only concern the somewhat trivial (doubly even, $T = 0$) ^{16}O and the $T = 1$ ^{18}O isotope and yield realistic values. The more sophisticated calculations of Chung [8]) with slightly modified Kuo-Brown matrix elements yield a poor value for ^{18}O but correctly predict the dipole moment for ^{20}O. This may not be too surprising since the matrix elements were fitted in the mass region $A = 18$–22. The calculation by Arima [9]), finally, concerns only ^{20}O and yields an unrealistically low value. In this paper a central residual interaction with a gaussian-shape radial dependende has been used.

TABLE 4

Magnetic moments of first-excited states of even O-isotopes

Isotope (I^π)	μ_{exp} [a]) (n.m.)	μ_{theor} (n.m.)
$^{16}O(3_1^-)$	$+1.65\pm0.09$ [b])	$+1.56$ [h])
	$+1.71\pm0.15$ [c])	
$^{18}O(2_1^+)$	-0.57 ± 0.03 [d])	-0.56 [h])
	-0.70 ± 0.08 [e])	-0.82 [i])
$^{20}O(2_1^+)$	-0.78 ± 0.08 [f])	-0.30 [j])
	-0.70 ± 0.03 [g])	-0.72 [i])

[a]) The signs are from refs. [22, 5, 10]) for ^{16}O, ^{18}O and ^{20}O, respectively.
[b]) Ref. [1]). [c]) Ref. [2]). [d]) Ref. [3]). [e]) Ref. [4]). [f]) Ref. [6]).
[g]) Present work.
[h]) Ref. [7]). [i]) Ref. [8]). [j]) Ref. [9]).

Clearly, better calculations are needed to reproduce the magnetic dipole moments of three isotopes simultaneously. It is likely that for ^{18}O core excitations must be included, whereas for ^{20}O this may be unnecessary.

The mean lifetime τ determined by the present work to be $\tau = 10.7\pm0.4$ ps is in good agreement with the value measured with Doppler-shift attenuation [$\tau = 9.8\pm0.7$ ps; see ref. [11])], but is more precise. The present value disagrees significantly, however, from that of a previous recoil-distance experiment [6]), which yielded $\tau = 14.2\pm0.8$ ps, a discrepancy which is discussed in the introduction.

The present experimental value leads to a single-particle strength of $M^2(E2) = 1.76\pm0.07$ W.u. for the $2_1^+ \rightarrow 0_1^+$ γ-ray transition. The value calculated by Arima [9]) amounts to $M^2(E2) = 1.68$ W.u. The agreement with experiment is, however, fortuitous since the 2_1^+ wave function of Arima cannot be correct; see above. A calculation based on the Chung wave functions [8]) for the 2_1^+ and 0_1^+ states yields

a single-particle strength for the $2_1^+ \rightarrow 0_1^+$ transition of 1.7 W.u. for a neutron effective charge of $e_n = 0.6$. Although this charge is somewhat higher than commonly used in this mass region [i.e. $e_n \simeq 0.5$, a value that was also taken in the calculation of Arima *et al.* [9]); see above] it is not unreasonable in view of the available small configuration space.

We may thus conclude that of the presently known wave functions those of Chung describe the properties of $^{20}O(2_1^+)$ best.

We like to thank A. G. M. van Hees for calculating the $2_1^+ \rightarrow 0_1^+$ transition strength in ^{20}O.

This work was performed as part of the research programme of the "Stichting voor Fundamenteel Onderzoek der Materie" (FOM) with financial support from the "Nederlandse Organisatie voor Zuiver-Wetenschappelijk Onderzoek" (ZWO).

References

1) W. L. Randolph, N. Ayres de Campos, J. R. Beene, J. Burde, M. A. Grace, D. F. H. Start and R. E. Warner, Phys. Lett. **44B** (1973) 36
2) C. Broude, M. B. Goldberg, G. Goldring, M. Hass, M. J. Renan, B. Sharon, Z. Shkedi and D. F. H. Start, Nucl. Phys. **A215** (1973) 617
3) J. Asher, M. A. Grace, P. D. Johnston, J. W. Koen, P. M. Rowe and W. L. Randolph, J. of Phys. **G2** (1976) 477
4) K. H. Speidel, M. B. Goldberg, K. Hagemeyer, G. J. Kumbartzki, G. Goldring, Z. Shkedi, M. Schramm, G. Kraft and H. A. Doubt, Phys. Lett. **57B** (1975) 143
5) M. Forterre, J. Gerber, J. P. Vivien, M. B. Goldberg and K. H. Speidel, Phys. Lett. **55B** (1975) 59
6) Z. Berant, C. Broude, G. Engler, M. Hass, R. Levy and B. Richter, Nucl. Phys. **A243** (1975) 519
7) T. T. S. Kuo and G. E. Brown, Nucl. Phys. **85** (1966) 40
8) W. Chung, Ph.D. thesis (Michigan State University) 1976
9) A. Arima, M. Sakakura and T. Sebe, Nucl. Phys. **A170** (1971) 273
10) J. Gerber, M. B. Goldberg and K. H. Speidel, Phys. Lett. **60B** (1976) 338
11) J. Hermans, G. A. P. Engelbertink, L. P. Ekström, H. H. Eggenhuisen and M. A. van Driel, Nucl. Phys. **A284** (1977) 307
12) R. E. Horstman, J. L. Eberhardt, H. A. Doubt, C. M. E. Otten and G. van Middelkoop, Nucl. Phys. **A248** (1975) 291
13) A. J. Rutten *et al.*, to be published
14) T. K. Alexander and H. Bell, Nucl. Instr. **81** (1970) 22
15) J. B. Marion and F. C. Young, Nuclear reaction analysis (North-Holland, Amsterdam, 1968)
16) M. Leventhal, Nucl. Instr. **110** (1973) 343
17) R. Marrus, Nucl. Instr. **110** (1973) 333
18) I. A. Sellin, M. Brown, W. W. Smith and B. Donnally, Phys. Rev. **A2** (1970) 1189
19) H. Kopfermann, Kernmomente (Akademischer Verlag, Frankfurt, 1956)
20) H. A. Doubt, in Atomic physics in nuclear experiments, ed. B. Rosner and R. Kalish (Adam Hilger, Bristol, 1977) p. 537
21) F. Ajzenberg-Selove, Nucl. Phys. **A300** (1978) 1
22) R. Kalish, M. Hass, J. M. Brennan and H. T. King, Nucl. Phys. **A276** (1977) 339